Sensors & Actuators: B. Chemical 331 (2021) 129458

Contents lists available at ScienceDirect

Sensors and Actuators: B. Chemical

journal homepage: www.elsevier.com/locate/snb

CRISPR/Cas12a-Modulated fluorescence resonance energy transfer with nanomaterials for nucleic acid sensing

Xiaoxue Cheng [a,1], Yurong Yan [b,1], Xueping Chen [a], Jiaxin Duan [a], Decai Zhang [a], Tiantian Yang [a], Xiaolong Gou [a], Min Zhao [b], Shijia Ding [b], Wei Cheng [a,*]

[a] The Center for Clinical Molecular Medical Detection, The First Affiliated Hospital of Chongqing Medical University, Chongqing, 400016, PR China
[b] Key Laboratory of Clinical Laboratory Diagnostics (Ministry of Education), College of Laboratory Medicine, Chongqing Medical University, Chongqing, 400016, PR China

ARTICLE INFO

Keywords:
CRISPR/Cas12a
FRET
Fluorescence
Nanomaterials
DNA sensing

ABSTRACT

Cas12a shows great promise in DNA sensing applications due to its target-triggered collateral *trans*-cleavage activity. But the cleavage effect towards probes modified on nanomaterials is less understood. In this work, an analogy analysis is performed to explore the cleavage properties of Cas12a system on the surface of nanomaterials by using gold nanoparticles (AuNPs) and graphene oxide (GO). The fluorescence of FAM-tagged probes is quenched by nanomaterials due to fluorescence resonance energy transfer (FRET). The *trans*-cleavage activity of Cas12a was activated to promiscuously digest the single-stranded part of probes, thereby modulating FRET effect between FAM labels and nanomaterials. The results showed that GO had better quenching ability and Cas12a-induced fluorescence recovery than AuNPs, and the double-stranded DNA probe with staggered end can lead preferable *trans*-cleavage efficiency, proving low steric hindrance of nanomaterials and appropriate orientation of probes play critical roles in Cas12a-modulated FRET with nanomaterials. Then, by integrating Cas12a system and GO-based post-quenching strategy, a DNA biosensor was developed with extremely high fluorescence response and low initial background. It is expected that this work will be of particularly useful for investigation of the interaction between CRISPR/Cas proteins and nanomaterials, as well as developing CRISPR-based point-of-care (POC) diagnostic platforms.

1. Introduction

Development of rapid, cost-effective, and easy-to-use biosensing platforms for nucleic acid tests is vital in molecular diagnostics, food inspection, environmental monitoring, and etc [1–3]. Among numerous DNA assays, the fluorescence resonance energy transfer (FRET) based strategy is dominant owing to its inherent advantages of ease of operation, rapid response, low cost, high selectivity and sensitivity [4–6]. FRET is a process in which energy is transferred from an excited state donor fluorophore to a ground state acceptor or quencher, resulting in enhanced acceptor fluorescence or quenching of donor fluorophore [6]. In classic FRET-based DNA biosensing strategy, A hairpin DNA probe containing a fluorophore and a quencher is usually engineered to form FRET pair [7,8]. The binding of probe and its target changes the distances between the fluorophore and the quencher, resulting in fluorescence recovery.

With ultrahigh quenching ability, a variety of nanomaterials, such as graphene oxide (GO) [9], gold nanoparticles (AuNPs) [10], carbon nanotubes (SWNTs) [11] and metal-organic frameworks (MOFs) [12] have been harnessed as efficient quenchers in FRET-based biosensors. Although enhanced signal-to-noise (S/N) ratio and thermal stability have been realized by DNA-nanomaterial assembly, the ratio of target recognizing/binding and signal output keeps on 1:1 resulting in unfavorable sensitivity. To further increase the fluorescence signal gain, various isothermal amplification strategies, including exonuclease III-assisted target recycling [13], catalyzed hairpin assembly (CHA) [9] and hybridization chain reaction (HCR) [14] have been exploited to achieve signal amplification. However, these strategies still suffer from some major drawbacks, such as time-consuming, complicated probe design, and high nonspecific background. For example, Exo III catalyzes

* Corresponding author at: The First Affiliated Hospital of Chongqing Medical University, The Center for Clinical Molecular Medical detection, 1# youyi Road, Yuzhong District, Chongqing, 400016, PR China.
E-mail address: chengwei@hospital.cqmu.edu.cn (W. Cheng).
[1] These authors contributed equally to this work.

https://doi.org/10.1016/j.snb.2021.129458
Received 15 September 2020; Received in revised form 7 December 2020; Accepted 4 January 2021
Available online 8 January 2021

the gradual digest nucleotides from the 3′ termini of DNA probe after hybridization of the probe and target DNA to form a double-strand structure, thereby releasing of the target for DNA circuits [13]. This hydrolysis mechanism relies on DNA hybridization process, resulting in low cleavage efficiency and long turnover period. Therefore, an integrated biomolecular system that allows specific target DNA recognition and efficient signal amplification is still highly desired in development of FRET-based DNA sensing platforms.

Recently, RNA-mediated CRISPR-associated (Cas) systems as promising signal transduction and amplification elements have been proven useful in sequence-specific DNA/RNA targeting and detection applications [15]. Within the CRISPR/Cas family, the Cas12a protein, programmed with a single CRISPR RNA (crRNA), can recognize and cleave double-strands DNA (dsDNA) targets with single-base resolution through protospacer-adjacent motif (PAM) identification and Watson-Crick base pairing [16]. Remarkably, the specific binding of Cas12a-cRNA duplex and its DNA target results in a conformational change that unleashes promiscuous single-stranded DNA (ssDNA) degradation (at a rate of about 1200 cuts per second) [17]. This multi-turnover *trans*-cleavage effect dramatically increases the signal response of DNA detection technologies. Moreover, due to relatively easier design and synthesis of crRNA, Cas12a protein is now being promisingly exploited as a powerful tool in universal molecular diagnostic area [18–20]. In our previous work, we have investigated the *trans*-cleavage efficiency of Cas12a towards hairpin DNA and linear DNA on electrode interface detailedly [21]. However, the *trans*-cleavage property towards DNA probes modified on the surface of nanomaterials is less understood.

In this work, a comparative experiment is performed by using two typical nanomaterials functionalized with different DNA probes to study the nanoquenching properties and nanosurface cleavage capacity of Cas12a. Zero-dimensional AuNPs are chosen as the representative of spherical nanomaterials and two-dimensional GO as nanosheets due to their advantages of good water solubility, easiness for modification, high surface area and outstanding quenching ability for fluorophore [22,23]. The fluorescence of FAM-tagged DNA probes is quenched by AuNPs or GO due to the distance-dependent FRET effect when there was no target exist [24,25]. The *trans*-cleavage activity of Cas12a can be triggered to cleave the DNA probes while presence of target, modulating FRET effect between FAM labels and nanomaterials and releasing fluorescence signal. The results showed that GO had better quenching ability and signal recovery than AuNPs, and the dsDNA probe with staggered end can lead higher *trans*-cleavage efficiency than single-strand and hairpin DNA probes owing to appropriate orientation of probes and accessibility of Cas12a. Finally, taking advantage of the multi-turnover trans-cleavage activity of Cas12a and the superior quenching efficiency of GO, a DNA assay by using Cas12a-modulated FRET with GO is obtained with the advantages of rapidity, low-cost and high sensitivity, which can offer robust yet flexible approaches for DNA detection in resource-limited settings. We expect that this work will contribute to the investigation of the interaction between CRISPR/Cas proteins and nanomaterials, as well as the design of the next-generation of CRISPR-based diagnostic systems.

2. Experimental section

2.1. Materials and reagents

EnGen Lba Cas12a and NEBuffer 2.1 were acquired from New England Biolabs (Ipswich, MA UK). GO was obtained from Sigma-Aldrich (St Louis, USA). $HAuCl_4$ was acquired from Sinopharm Chem Co., Ltd (Shanghai, China). RNase inhibitor and crRNA were received from TaKara Bio Inc. (Dalian, China). The DNA oligonucleotides were purchased by Sangon Biotechnology Co., Ltd. (Shanghai, China). All the nucleotide sequences were shown in Table S1. TS and NTS were annealed in 10 × NEBuffer 2.1 at 37 °C for 30 min to form target dsDNA.

2.2. Apparatus

UV-2550 UV–vis spectrophotometer (Shimadzu, Japan) was used to record the UV–vis absorption spectra. Cary Eclipse Fluorescence Spectrophotometer (Agilent Technologies, USA) was utilized to obtain the fluorescence spectra. PYX-DHS-BS-II constant temperature incubator (Hengwell, China) was introduced to incubate all reactions. Bio-Rad electrophoresis analyzer (Bio-Rad, USA) and on Bio-Rad ChemDoc XRS (Bio-Rad, USA) were used for electrophoresis analysis.

2.3. Preparation and DNA-functionalization of AuNPs

AuNPs and its DNA functionalization were prepared according to the previously published work [26]. In briefly, sodium citrate (10.1 mL, 34 mM) was rapidly added to the boiling solution of HAuCl4 (88.2 mL, 1 mM), and the color of the mixed solution changed from pale yellow to deep red in 1 min. Then cooled the resulting AuNP solution to room temperature (RT) with uninterrupted stirring for another 20 min and stored at 4 °C for further use.

The DNA-modified AuNPs were acquired by incubating a mixture consisting of 49 μL of 100 μM thiol-functionalized DNA, 5 μL of 500 mM acetate buffer (pH 5.2) and 1.5 μL of 10 mM TCEP at RT for 1 h. Then 1.6 mL of the AuNP solution was added into the mixture, and the resulting solution was stored in a drawer at RT for at least 16 h. Then, 20 μL of 400 mM Tris-acetate buffer (pH 8.2) was added to the mixture drop by drop, and 160 μL of 1 M NaCl was added to the mixture dropwise. Subsequently, the resulting solution was stored in a drawer for at least 12 h. Finally, the mixture was centrifuged (15000 rpm, 20 min) to remove the excess reagents. Equal p-DNA was added into c-DNA(SH)-functionalized AuNPs in hybridization buffer (100 mM NaCl, 100 mM KCl, 50 mM Tris-HCl, pH 7.4) and further incubated at RT for 1 day. Then, the excess DNA was removed after centrifugation (15000 rpm, 20 min). Finally, the red solution was stored at 4 °C in dark for further use.

2.4. Fluorescent analysis

For GO-based FRET assay, 50 μL of solution 1 was obtained by mixing up 2 μL of 20 μM probes, 16 μL of 1 mg/mL GO and 5 μL 10×NEBuffer 2.1 for 10 min at RT. 5 μL of 200 nM Cas12a, 5 μL of 200 nM crRNA and 5 μL of 20 U/μL RNase Inhibitor were applied for assembling Cas-crRNA complex at RT for 10 min. After that, 50 μL solution 2 was acquired by adding 20 μL target dsDNA to pre-assembled Cas-crRNA complex for 10 min at RT. Finally, solution 1 and solution 2 were mixed for brief vortex and further incubated at 37 °C for 1 h, followed by fluorescent measurements.

For AuNPs-based FRET assay, 50 μL of DNA probes/AuNPs were centrifuged (12000 rpm, 20 min) to remove the supernatant and resuspended with 1×NEBuffer 2.1. Solution 2 was assembled as above mention. The two solutions were mixed and for brief vortex, and the result solution was further incubated in 37 °C for 1 h, followed by fluorescent measurements.

All the fluorescence spectra were recorded from 500 nm to 600 nm with the excitation wavelength of 492 nm and the voltage of 600 V. Both the silt widths of excitation and emission were 5 nm.

2.5. Native polyacrylamide gel electrophoresis

To confirm the *trans*-cleavage ability of Cas12a, the products and components of Cas12a were studied with 12 % native polyacrylamide gel electrophoresis (PAGE) in 1 × TBE running buffer (89 mM Tris-boric acid, 2 mM EDTA, pH 8.3) at 120 V constant voltage for 40 min. the gels were imaged using gel image system after Gold view (GV) staining for 20 min. The total volume of every lane is 20 μL and the final concentration of each components are as follows: 0.5 U/μL RNase inhibitor, 250 nM Cas12a, 500 nM crRNA, 1×NEBuffer 2.1, 500 nM Target,

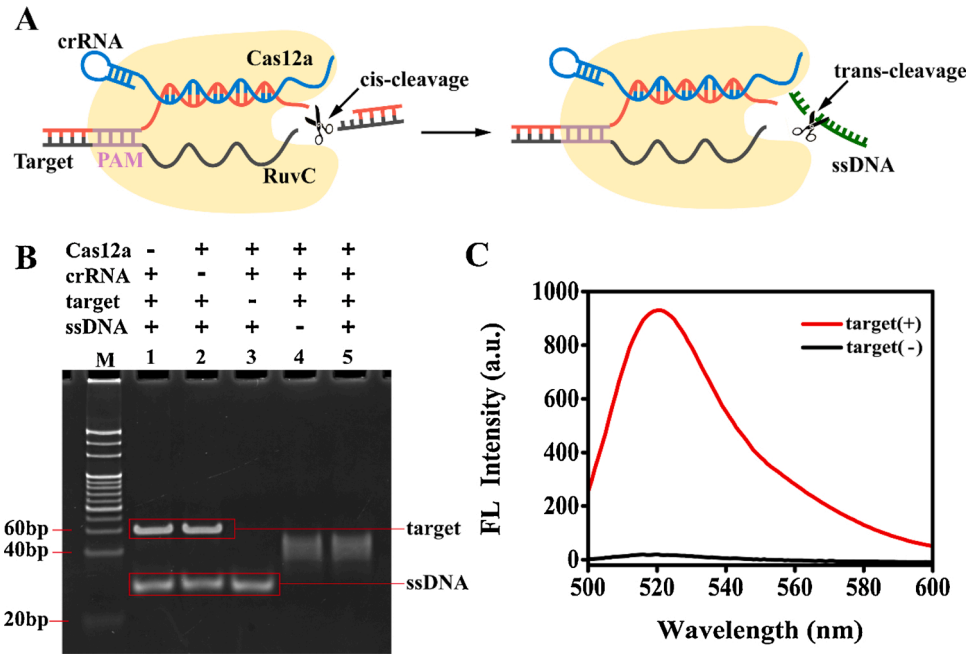

Fig. 1. (A) Schematic illustration of the *cis*- and *trans*-cleavage activities of Cas12a. (B) 12 % PAGE analysis of the Cas12a-mediated substrate cleavage. (C) Fluorescence spectra of Cas12a-mediated FQ probe cleavage (λex 492 nm, λem 520 nm).

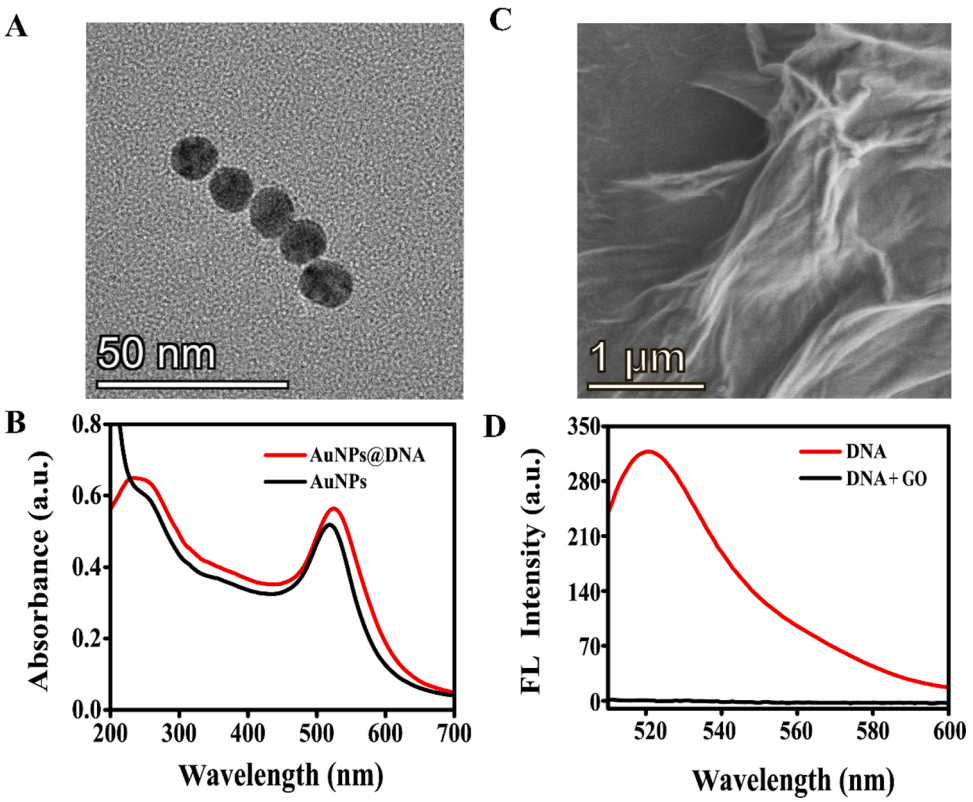

Fig. 2. (A) TEM image of AuNPs used in this work. (B) UV–vis spectra of AuNPs (black) and DNA-modified AuNPs (red). (C) TEM image of GO used in this work. (D) Fluorescence spectra of FAM-modified probe before (red) and after (black) the addition of GO (λex492 nm, λem 520 nm).

500 nM ssDNA probe(A 20).

3. Results and discussion

3.1. Characterization of Cas12a-mediated trans-cleavage activity

Recent studies have showed that Cas12a system has both precise *cis*-cleavage activity and nonspecific *trans*-cleavage activity related to the

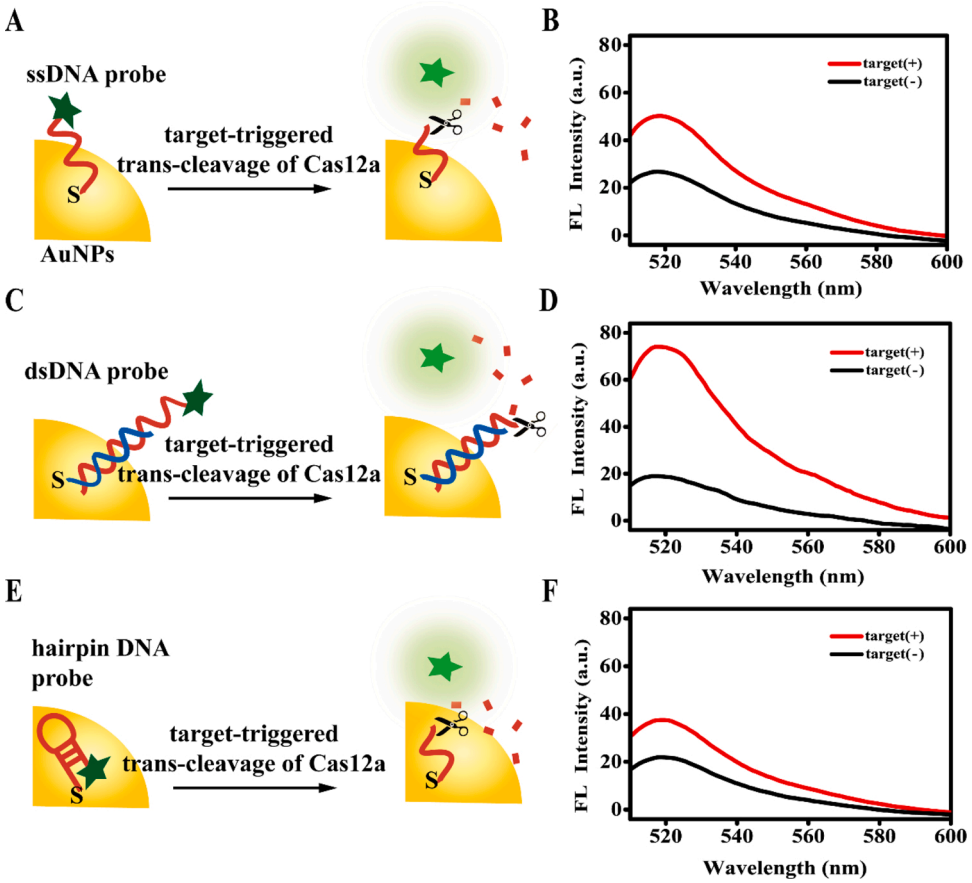

Fig. 3. Schematic illustration of Cas12a-modulated FRET based on AuNPs and three types of DNA probes (A, C and E) and fluorescence spectra of Cas12a acting on the three probes (B, D and F) (λex 492 nm, λem 520 nm).

catalytic domain of RuvC [27,28]. As illustrated in Fig. 1A, Cas12a can bind with crRNA to form a Cas12a-crRNA complex. Subsequently, the Cas12a-crRNA complex recognizes a short T-rich protospacer- adjacent motif (PAM) in dsDNA target and unwinds the target to form a DNA/RNA heteroduplex, leading the conformation rearrangement to expose RuvC pocket. The *cis*-cleavage activity is triggered to break dsDNA with staggered ends. Then the PAM-distal digestion products are released from the RuvC pocket, enabling nonspecific ssDNA substrates access and cleavage. To verify the *trans*-cleavage activity of Cas12a, a nonspecific ssDNA was employed as the degradation substrate. The 12% PAGE analysis was carried out to characterize the cleavage products. As shown in Fig. 1B, the Cas12a-crRNA duplex could specifically recognize and cleave target dsDNA (lane 4). After the *cis*-cleavage ability of Cas12a was activated, the nonspecific ssDNA substrates were completely cleaved (lane 5), presenting that the *trans*-cleavage activity of Cas12a was highly activated. The fluorophore quencher (FQ)-labeled probes were further introduced into the Cas12a-mediated ssDNA degradation process. The results indicated that the FQ probes could be efficiently digested and release significant fluorescence (Fig. 1C). Above consistent results confirmed that Cas12a can be successfully introduced into fluorescent DNA assay as a powerful biorecognition and transduction element.

3.2. Characterization and functionalization of nanomaterials

Transmission electron microscopy (TEM) was employed to characterize the size and morphology of AuNPs and GO. The AuNPs presented good dispersion status and relatively uniform sphericity structure, and the average size of the nanoparticles was measured to be ~14 nm (Fig. 2A). Although different size had diverse fluorescence quenching efficiency, this most common used size was just adopted as the model of particle nanomaterials [29]. Meanwhile, the DNA functional AuNPs were further studied by UV–vis spectra. It is observed that the unmodified AuNPs had a sharp peak at 520 nm. The characteristic peak of AuNPs was slightly red shifted after DNA modification and nucleic peak appeared at the 260 nm, indicating that DNA probe was successfully modified on AuNPs surface (Fig. 2B). As displayed in Fig. 2C, the GO used in this work had large size more than several micrometers with sheet structure. The quenching ability of GO was characterized by fluorescence spectroscopy. The results exhibited that the fluorescence of probes could be completely quenched by GO, indicating that GO had affinity towards ssDNA and could be used as a super nanoquencher (Fig. 2D).

3.3. Cleaving DNA probes on AuNPs

To investigate the quenching ability of AuNPs and cleavage efficiency of Cas12a on AuNPs surface, a comparative study is performed by using three types of DNA probes (ssDNA, dsDNA with staggered end, and hairpin DNA probes) with 5′ -FAM and 3′ -thiol labeled (Fig. 3A, C and E). For the dsDNA with staggered end group, the around 8 nm of distance between FAM and surface of AuNPs was chosen as an optimized distance to obtain a strong quenching efficiency referring to Chhabra 's research [29]. The three probes were modified to AuNPs surface through S-Au bonding and the ratio of probes to AuNPs was studied to achieve the optimized packing density (Fig. S2). As shown in Fig. 3B, D and F, the fluorescence of the three probes was highly quenched by AuNPs in the absence of the target DNA, resulting in similar low fluorescence intensity (FL intensity). When the *trans*-cleavage of Cas12a was triggered by target DNA, fluorescence was restored owing to the

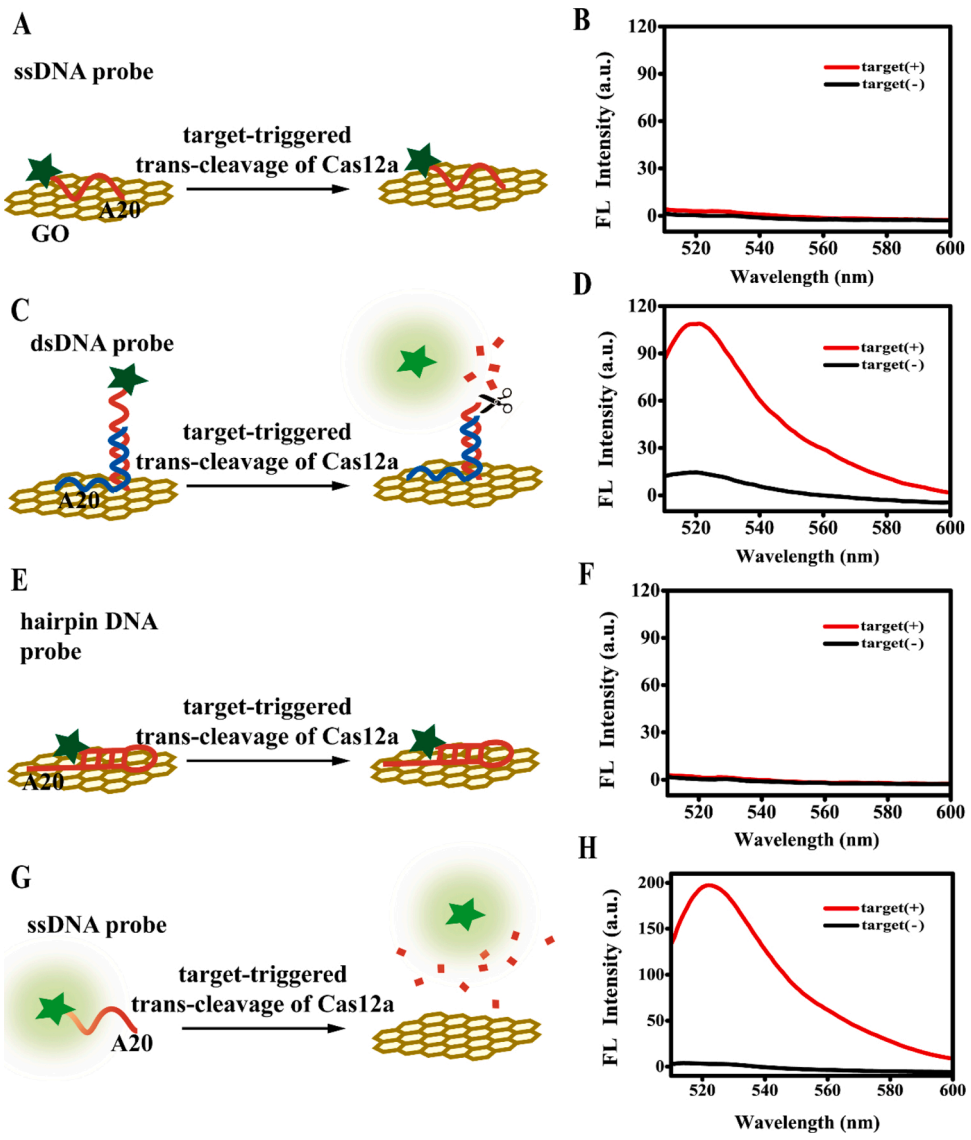

Fig. 4. Schematic illustration of Cas12a-mudulated FRET based on GO and three types of DNA probes (A, C, E and G) and fluorescence spectra of Cas12a acting on the three probes (B, D, F and H) (λex 492 nm, λem 520 nm).

degradation of the ssDNA part of the probes, proving the feasibility of Cas12a modulating FRET effect on AuNPs surface. It should be observed that dsDNA probe had better fluorescence signal recovery, while ssDNA and hairpin DNA probe had relatively low fluorescence signal. The low fluorescence recovery rate of ssDNA probes might be attributed to the formation of high-density DNA monolayer on AuNPs through strong ssDNA-AuNPs interaction. The previous report had already noted the hairpin DNA formed DNA-AuNPs composite had a similar hydrodynamic diameter with ssDNA-AuNPs composite [30], suggesting that the hairpin probe might lay on the surface of AuNPs like ssDNA probe instead of standing up. Therefore, for ssDNA and hairpin DNA probes, the relatively high DNA density on AuNPs surface resulted in high steric hindrance effect and poor accessibility of Cas12a towards probes. The dsDNA modified AuNPs showed a bigger hydrodynamic diameter because of the rigid double helical conformation of dsDNA [30], providing incompact morphological structure and appropriate orientation. Furthermore, since the 5′ flap of dsDNA probe was a single stranded overhang, this flap structure was distinctively utilized as cleavage site for activated-Cas12a (Fig. 3B). Further, dsDNA group with best signal response is chosen as model to further modulate the surface probe density by using short thiol modified "helper" strand [31]. As Fig. S2 illustrated, different probe density could indeed influence the *trans*--cleavage of Cas12a.When the ratio of "helper" strand to dsDNA probe is 2:1, the fluorescence response was higher than the completely dsDNA probe group.

3.4. Cleaving DNA probes on GO

A 20-base polyadenine (A_{20}) was used to replace thiol group of the above three probes, which could attach these probes to the surface of GO due to π-π stacking between adenine and GO (Fig. 4A, C, E and G) [12, 32]. As shown in Fig. 4B and F, the fluorescence of ssDNA and hairpin DNA probes were nearly totally quenched by GO, indicating that the quenching ability of GO is higher than that of AuNPs, which coincided with previous report [33]. In contrast, the quenching ability of GO for dsDNA probe is slightly lower than that of ssDNA and hairpin DNA probes, which could be due to the longer distance between GO surface and the FAM labels of rigid dsDNA (Fig. 4D) [34]. It should be noted that only the dsDNA probe restored fluorescence after the cleavage of activated-Cas12a. For ssDNA probe, Cas12a could not cleave it due to the probe completely adhered on the surface of GO through π-π stacking (Fig. 4A and B). The structure of dsDNA with tail was used to make probe

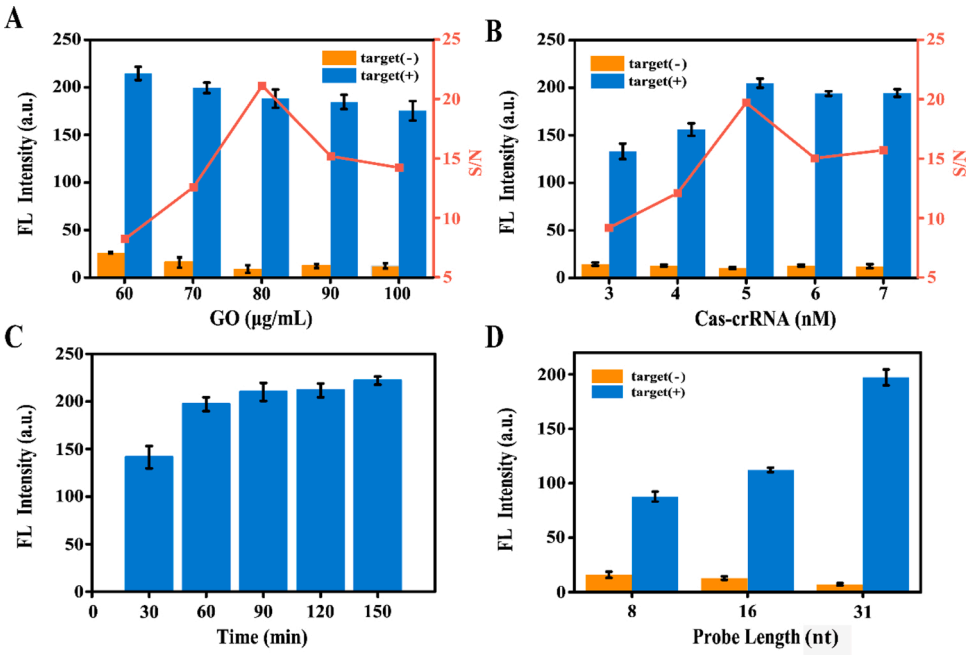

Fig. 5. The optimization of concentration of GO (A) and Cas12a-crRNA (B), reaction time (C), and probe length (D). Error bars represent standard derivation obtained in three parallel experiments.

absorbed on the surface of GO and fluorescein away from the surface of GO to make probe be easily cleaved by Cas12a [5]. Subsequently target trigged-Cas12a could cleave the 5′ flap of dsDNA probe to unleash the fluorescence (Fig. 4C and D). Varying the structure of probe to hairpin, in which FAM was closer to the surface of GO than dsDNA probe, could meet the purpose of lower background signal. However, the fluorescence spectrum showed that hairpin DNA probe had almost no signal recovery (Fig. 4E and F), which could be attributed to the strong affinity between GO and ssDNA (the loop portion and the A_{20} tail) pulling the hairpin probe lay on the GO surface like ssDNA probe [35]. These results further demonstrated that dsDNA modified on the GO surface was more susceptible to be cleaved by Cas12a. Comparing with AuNPs group, much higher fluorescence signal was obtained because of the excellent nucleic acid load due to remarkable surface area of GO.

In addition, to avoid the influence of steric hindrance effect on the *trans*-cleavage efficiency of Cas12a, a post-quenching strategy was performed by changing the adding order of ssDNA probe and GO (Fig. 4G). As it can be clearly seen in Fig. 4H, an extremely high fluorescence signal and low initial background were obtained, making S/B ratio significantly higher than that of the above pre-quenching strategies. It was worthy to mention that the fluorescence signal of this post-quenching strategy was still a bit lower than the FQ probe due to steric hindrance and modification efficiency (Fig. S4). These results of AuNPs and GO indicated that steric hindrance effect of nanomaterials and appropriate orientation of DNA probes significantly influenced the *trans*-cleavage efficiency of Cas12a at interface, thereby affects the analytical performance of the designed technologies. Thus, the post-quenching strategy was chosen for developing Cas12a-Modulated FRET with GO.

3.5. Optimization of experimental conditions

Several important experimental conditions were further optimized to improve the analytical performance for DNA detection with post-quenching strategy of GO. Firstly, the influence of GO concentration on fluorescence quenching efficiency was investigated. As shown in Fig. 5A, the FL intensity for the positive sample decreased with the increasing of the concentration of GO. The S/B ratio reached a maximum value at 80 μg/mL, which was then chosen as the optimal concentration. The *trans*-cleavage process of Cas12a could be affected by the concentration of Cas12a-crRNA complex and the reaction time. As depicted in Fig. 5B, the FL intensity increased until the concentration of Cas12a-crRNA complex exceeded 5 nM in the present of the target. In

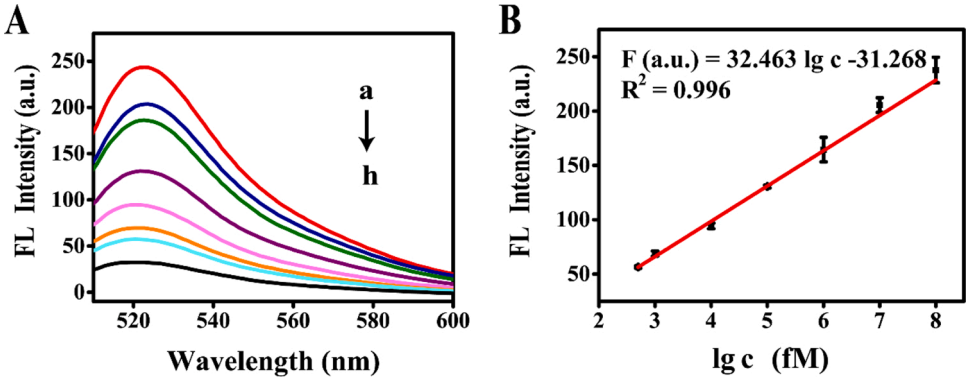

Fig. 6. (A) Typical fluorescence spectra curves responding to 10^8, 10^7, 10^6, 10^5, 10^4, 10^3, 500, and 0 fM of target DNA (from a to h). (B) The calibration curve for the FL intensity versus the logarithm of target DNA. Error bars represent standard derivation obtained in three parallel experiments.

Table 1
Comparison between the Cas12a-Modulated GO FRET strategy and other reported FRET-based methods for nucleic acids detection.

Target	Donor/ accepter	Amplification Method*	Line range (nM)	LOD (nM)	Refs.
RNA	FAM/GO	–	–	24	[35]
DNA	Cy3/GO	–	5–75	1	[36]
DNA	AIE/GO	–	0–100	2.5	[37]
DNA	AgNCs/ GO	HCR	10–100	1.18	[38]
miRNA	QDs/GO	EDC	1×10^{-3}-1	1×10^{-3}	[39]
RNA	FAM/GO	ETR	0–30	2×10^{-2}	[40]
miRNA	FAM/GO	ETR	0.5-1	1.6×10^{-4}	[41]
miRNA	FAM/GO	RCA	1×10^{-6}-5×10^{-2}	4×10^{-4}	[42]
DNA	FAM/GO	Cas12a	5×10^{-4}-100	1.34×10^{-4}	This work

* HCR: hybridization chain reaction. EDC: enzyme-free DNA circuits. ETR: enzyme-aided target recycling. RCA: rolling circle amplification.

contrast, there was no obvious change for the FL intensity of the blank sample. So, 5 nM was selected for the subsequent experiments. Then, the cleavage period was evaluated from 30 to 150 min (Fig. 5C). The FL intensity increased slowly after 60 min, so 60 min was chosen as the appropriate reaction time. In addition, the length of the ssDNA probe is another important factor. Fig. S3 showed the fluorescence of ssDNA probe was quenched quickly after adding GO and reached equilibrium in 5 min, indicating that time of 5 min was sufficient for the incubation of GO. In addition, the length of the ssDNA probe was also investigated. As can be seen from Fig. 5D, for a long ssDNA probe (31 nt), they gave a relatively low background signal, but the FL intensity of the positive sample increased significantly, indicating that long ssDNA might have stronger adsorption with GO [34], and Cas12a might be more accessible to long ssDNA.

3.6. Analytical performance

Under optimized experimental conditions, the analytical performance of the Cas12a-Modulated GO FRET biosensor was evaluated. As displayed in Fig. 6A, the FL intensity gradually increased with the increasing of target DNA concentrations. Fig. 6B showed the FL intensity and the logarithm of target DNA concentration existed a good linear correlation in the range from 500 fM to 100 nM. The regression equation was F (a.u.) = 32.463 lg c – 31.268 with a correlation coefficient (R^2) of 0.996, where F was the FL intensity and c was the concentration of target DNA. The limit of the detection (LOD) was calculated to be 134 fM according to the 3 σ rule, which was superior to those of reported GO-based FRET biosensors for nucleic acids detection (Table 1). The high sensitivity and wide linear range of the Cas12a-Modulated GO FRET strategy was attributed to the superior quenching efficiency of GO and the multi-turnover *trans*-cleavage activity of Cas12a.

3.7. Interference assay

To further investigate the applicability and specificity of the method for detecting target DNA in complicated DNA extracts, Fluorescence signal was evaluated by spiking target DNA with different concentration in 0.1 μg/mL total DNA extracted from vaginal/anal swabs of healthy women volunteers. As Fig.7 A depicted, the fluorescence signals decreased a little in total DNA extracts due to the interference of the sample matrix during the target triggered cleavage reaction. However, the FL intensity of target in DNA extracts group possessed a good target concentration-dependent decrease. Fig. 7B displayed the comparison of the peak F-F_0 intensity of target DNA with different concentration in water and total DNA extracts under the same experimental condition. It could be seen that even 1 pM of target DNA in 0.1 μg/mL total DNA extracts was still obviously detected. The results indicated the applicability of the established system for target DNA detection in complicated real sample.

4. Conclusion

In this work, an analogy analysis is performed by using GO/AuNPs with different structural DNA probes to explore the nanoquenching abilities and the cleavage properties of Cas12a on nanomaterials. It was approved that GO had better quenching ability and fluorescence recovery than AuNPs, and the double-stranded DNA probe with staggered end can lead preferable trans-cleavage efficiency due to incompact morphological structure and appropriate orientation. In addition, the post-quenching strategy could avoid the influence of steric hindrance, thus obtaining a higher S/B ratio. Consequently, the Cas12a-Modulated GO FRET biosensor is developed by combining Cas12a system and GO-based post-quenching strategy for DNA detection. More importantly, the programmability of crRNA provides a versatile analytical platform as the proposed assay can be applied to detect any target DNA. On the premise of rapidity, cost-effectiveness, and high sensitivity, the Cas12a-Modulated GO FRET biosensor can offer robust yet flexible approaches for POC testing applications. Compared to FQ probes, the sensitivity of Cas12a-based cleavage towards probes modified on nanomaterials really need to be improved due to steric hindrance and modification efficiency. However, the proposed strategy can also be combined with other isothermal amplification methods to construct higher sensitive biosensor in the future. We expect that this work will provide guidance for the study of the interactions between CRISPR and nanomaterials, as well as for the design of new CRISPR-based diagnostic systems.

CRediT authorship contribution statement

Xiaoxue Cheng: Conceptualization, Methodology, Software, Investigation, Data curation, Writing - original draft. **Yurong Yan:** . **Xueping Chen:** . **Jiaxin Duan:** Methodology, Software, Investigation, Project administration, Writing - review & editing. **Decai Zhang:** Software,

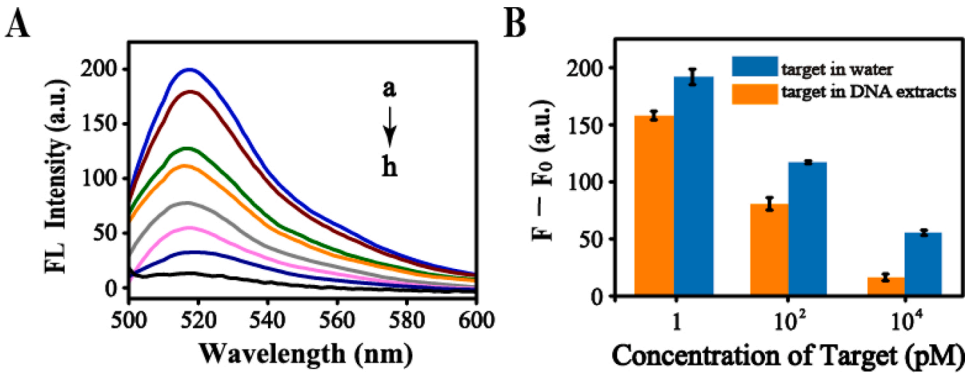

Fig. 7. (A) Fluorescence spectra of 10^4 pM target in water (a) and in 0.1 μg/mL total DNA extracts (b), 10^2 pM target in water (c) and in 0.1 μg/mL total DNA extracts (d), 1 pM target in water (e) and in 0.1 μg/mL total DNA extracts (f) and 0 pM target in water (g) and in 0.1 μg/mL total DNA extracts (h). (B) Comparison of different concentration of target DNA (10^4, 10^2 and 1 pM) prepared with water and DNA extracts. Error bars represent standard derivation obtained in three parallel experiments.

Investigation, Project administration. **Tiantian Yang:** Formal analysis, Software. **Xiaolong Gou:** Resources, Software. **Min Zhao:** Resources, Software. **Shijia Ding:** Supervision, Methodology, Data curation, Project administration. **Wei Cheng:** Funding acquisition, Supervision, Project administration, Data curation.

Declaration of Competing Interest

The authors report no declarations of interest.

Acknowledgements

This work was funded by the National Natural Science Foundation of China (81873980 and 81873972), the Chongqing Science Fund for Distinguished Young Scholars (cstc2019jcyjjqX0028) and the Training Program for Advanced Young Medical Personnel of Chongqing (2017HBRC003).

Appendix A. Supplementary data

Supplementary material related to this article can be found, in the online version, at doi:https://doi.org/10.1016/j.snb.2021.129458.

References

[1] Y. Liu, Y.M. Wang, W.Y. Zhu, C.H. Zhang, H. Tang, J.H. Jiang, Conjugated polymer nanoparticles-based fluorescent biosensor for ultrasensitive detection of hydroquinone, Anal. Chim. Acta 1012 (2018) 60–65.
[2] A.J. Vargas, C.C. Harris, Biomarker development in the precision medicine era: lung cancer as a case study, Nat. Rev. Cancer 16 (2016) 525–537.
[3] W. Xu, Y. Xiong, W. Lai, Y. Xu, C. Li, M. Xie, A homogeneous immunosensor for AFB1 detection based on FRET between different-sized quantum dots, Biosens. Bioelectron. 56 (2014) 144–150.
[4] W.R. Algar, N. Hildebrandt, S.S. Vogel, I.L. Medintz, FRET as a biomolecular research tool - understanding its potential while avoiding pitfalls, Nat. Methods 16 (2019) 815–829.
[5] F. Tian, J. Lyu, J. Shi, M. Yang, Graphene and graphene-like two-denominational materials based fluorescence resonance energy transfer (FRET) assays for biological applications, Biosens. Bioelectron. 89 (2017) 123–135.
[6] X. Zhang, Y. Hu, X. Yang, Y. Tang, S. Han, A. Kang, et al., FOrster resonance energy transfer (FRET)-based biosensors for biological applications, Biosens. Bioelectron. 138 (2019) 111314.
[7] A. Moutsiopoulou, D. Broyles, E. Dikici, S. Daunert, S.K. Deo, Molecular aptamer beacons and their applications in sensing, imaging, and diagnostics, Small. 15 (2019), e1902248.
[8] J. Zheng, R. Yang, M. Shi, C. Wu, X. Fang, Y. Li, et al., Rationally designed molecular beacons for bioanalytical and biomedical applications, Chem. Soc. Rev. 44 (2015) 3036–3055.
[9] S.J. Zhen, X. Xiao, C.H. Li, C.Z. Huang, An enzyme-free DNA circuit-assisted graphene oxide enhanced fluorescence anisotropy assay for MicroRNA detection with improved sensitivity and selectivity, Anal. Chem. 89 (2017) 8766–8771.
[10] X. Miao, Z. Cheng, H. Ma, Z. Li, N. Xue, P. Wang, Label-free platform for MicroRNA detection based on the fluorescence quenching of positively charged gold nanoparticles to silver nanoclusters, Anal. Chem. 90 (2018) 1098–1103.
[11] C. Farrera, F. Torres Andon, N. Feliu, Carbon nanotubes as optical sensors in biomedicine, ACS Nano 11 (2017) 10637–10643.
[12] H.S. Wang, H.L. Liu, K. Wang, Y. Ding, J.J. Xu, X.H. Xia, et al., Insight into the unique fluorescence quenching property of metal-organic frameworks upon DNA binding, Anal. Chem. 89 (2017) 11366–11371.
[13] R.A. Xiaoqing Liu, Ronit Freeman, Omer Yehezkeli, Itamar Willner, Multiplexed aptasensors and amplified DNA sensors using functionalized graphene oxide: application for logic gate operations, ASC Nano 6 (2012) 3553–3563.
[14] J. Guo, C. Mingoes, X. Qiu, N. Hildebrandt, Simple, amplified, and multiplexed detection of MicroRNAs using time-gated FRET and hybridization chain reaction, Anal. Chem. 91 (2019) 3101–3109.
[15] Y. Li, S. Li, J. Wang, G. Liu, CRISPR/Cas systems towards next-generation biosensing, Trends Biotechnol. 37 (2019) 730–743.
[16] B. Zetsche, J.S. Gootenberg, O.O. Abudayyeh, I.M. Slaymaker, K.S. Makarova, P. Essletzbichler, et al., Cpf1 is a single RNA-guided endonuclease of a class 2 CRISPR-Cas system, Cell 163 (2015) 759–771.
[17] E.M.Janice S. Chen, Lucas B. Harrington, Maria Da Costa, Xinran Tian, Joel M. Palefsky, Jennifer A. Doudna, CRISPR-Cas12a target binding unleashes indiscriminate single-stranded DNase activity, Science 360 (2018) 436–439.
[18] Y. Xiong, J. Zhang, Z. Yang, Q. Mou, Y. Ma, Y. Xiong, et al., Functional DNA regulated CRISPR-Cas12a sensors for point-of-care diagnostics of non-nucleic-acid targets, J. Am. Chem. Soc. 142 (2020) 207–213.
[19] M. Liang, Z. Li, W. Wang, J. Liu, L. Liu, G. Zhu, et al., A CRISPR-Cas12a-derived biosensing platform for the highly sensitive detection of diverse small molecules, Nat. Commun. 10 (2019) 3672.
[20] Y. Dai, R.A. Somoza, L. Wang, J.F. Welter, Y. Li, A.I. Caplan, et al., Exploring the trans-cleavage activity of CRISPR-Cas12a (cpf1) for the development of a universal electrochemical biosensor, Angew. Chem. Int. Ed. Engl. 58 (2019) 17399–17405.
[21] D. Zhang, Y. Yan, H. Que, T. Yang, X. Cheng, S. Ding, et al., CRISPR/Cas12a-mediated interfacial cleaving of hairpin DNA reporter for electrochemical nucleic acid sensing, ACS Sens. 5 (2020) 557–562.
[22] S. Sajjad, S.A. Khan Leghari, A. Iqbal, Study of graphene oxide structural features for catalytic, antibacterial, gas sensing, and metals decontamination environmental applications, ACS Appl. Mater. Interfaces 9 (2017) 43393–43414.
[23] F. Zhang, S. Wang, J. Liu, Gold nanoparticles adsorb DNA and aptamer probes too strongly and a comparison with graphene oxide for biosensing, Anal. Chem. 91 (2019) 14743–14750.
[24] H. Zhang, H. Zhang, A. Aldalbahi, X. Zuo, C. Fan, X. Mi, Fluorescent biosensors enabled by graphene and graphene oxide, Biosens. Bioelectron. 89 (2017) 96–106.
[25] J.E. Kim, J.H. Choi, M. Colas, D.H. Kim, H. Lee, Gold-based hybrid nanomaterials for biosensing and molecular diagnostic applications, Biosens. Bioelectron. 80 (2016) 543–559.
[26] H.D. Hill, C.A. Mirkin, The bio-barcode assay for the detection of protein and nucleic acid targets using DTT-induced ligand exchange, Nat. Protoc. 1 (2006) 324–336.
[27] D.C. Swarts, M. Jinek, Mechanistic Insights into the cis- and trans-Acting DNase Activities of Cas12a, Mol. Cell 73 (2019) 589–600, e4.
[28] D.C. Swarts, J. van der Oost, M. Jinek, Structural basis for guide RNA processing and seed-dependent DNA targeting by CRISPR-Cas12a, Mol. Cell 66 (2017) 221–233, e4.
[29] R. Chhabra, J. Sharma, H. Wang, S. Zou, S. Lin, H. Yan, et al., Distance-dependent interactions between gold nanoparticles and fluorescent molecules with DNA as tunable spacers, Nanotechnology 20 (2009), 485201.
[30] A.C. Wong, D.W. Wright, Size-dependent cellular uptake of DNA functionalized gold nanoparticles, Small 12 (2016) 5592–5600.
[31] J. Zhang, L. Wang, H. Zhang, F. Boey, S. Song, C. Fan, Aptamer-based multicolor fluorescent gold nanoprobes for multiplex detection in homogeneous solution, Small 6 (2010) 201–204.
[32] B. Liu, S. Salgado, V. Maheshwari, J. Liu, DNA adsorbed on graphene and graphene oxide: fundamental interactions, desorption and applications, Curr. Opin. Colloid Interface Sci. 26 (2016) 41–49.
[33] F. Li, H. Pei, L. Wang, J. Lu, J. Gao, B. Jiang, et al., Nanomaterial-based fluorescent DNA analysis: a comparative study of the quenching effects of graphene oxide, carbon nanotubes, and gold nanoparticles, Adv. Funct. Mater. 23 (2013) 4140–4148.
[34] P.J. Huang, J. Liu, DNA-length-dependent fluorescence signaling on graphene oxide surface, Small. 8 (2012) 977–983.
[35] M. Stobiecka, B. Dworakowska, S. Jakiela, A. Lukasiak, A. Chalupa, K. Zembrzycki, Sensing of survivin mRNA in malignant astrocytes using graphene oxide nanocarrier-supported oligonucleotide molecular beacons, Sens. Actuators B Chem. 235 (2016) 136–145.
[36] L. Tang, D. Li, J. Li, Formation of a graphene oxide-DNA duplex-based logic gate and sensor mediated by RecA-ssDNA nucleoprotein filaments, Chem Commun. 49 (2013) 9971–9973.
[37] S. Zhang, K. Wang, K.B. Li, W. Shi, W.P. Jia, X. Chen, et al., A DNA-stabilized silver nanoclusters/graphene oxide-based platform for the sensitive detection of DNA through hybridization chain reaction, Biosens. Bioelectron. 91 (2017) 374–379.
[38] R. Huang, Y. Liao, X. Zhou, Y. Fu, D. Xing, Multiplexed detection of microRNA biomarkers from tumor cells and tissues with a homogeneous nano-photon switch, Sens. Actuators B Chem. 247 (2017) 505–513.
[39] A. Tyagi, K.L. Chu, I.H. Abidi, A.A. Cagang, Q. Zhang, N.L.C. Leung, et al., Single-probe multistate detection of DNA via aggregation-induced emission on a graphene oxide platform, Acta Biomater. 50 (2017) 334–343.
[40] Y. Ning, L. Zou, Q. Gao, J. Hu, F. Lu, Graphene oxide-based fluorometric determination of methicillin-resistant Staphylococcus aureus by using target-triggered chain reaction and deoxyribonuclease-assisted recycling, Mikrochim. Acta 185 (2018) 183.
[41] S. Guo, F. Yang, Y. Zhang, Y. Ning, Q. Yao, G.-J. Zhang, Amplified fluorescence sensing of miRNA by combination of graphene oxide with duplex-specific nuclease, Anal. Methods 6 (2014) 3598–3603.
[42] C. Hong, A. Baek, S.S. Hah, W. Jung, D.E. Kim, Fluorometric detection of MicroRNA using isothermal gene amplification and graphene oxide, Anal. Chem. 88 (2016) 2999–3003.

Xiaoxue Cheng is currently a graduate student of Chongqing Medical University majoring in clinical laboratory diagnosis. Her research interest is the development of biosensing strategy for clinical diagnosis.

Yurong Yan received Ph.D. degree from Chongqing Medical University in 2008, and became an associate professor of Chongqing Medical University in 2008. Her research interests focus on electrochemical and surface plasmon resonance biosensors and nanobiotechnology.

Xueping Chen is currently a doctor of in The Center for Clinical Molecular Medical detection, The First Affiliated Hospital of Chongqing Medical University. His research interest is the development of biosensing strategy for clinical laboratory diagnosis.

Jiaxin Duan is currently a graduate student of Chongqing Medical University majoring in clinical laboratory diagnosis. Her research interest is the development of biosensing strategy for clinical diagnosis.

Decai Zhang is currently a graduate student of Chongqing Medical University majoring in clinical laboratory diagnosis. His research interest is the development of biosensing strategy for clinical diagnosis.

Tiantian Yang is currently a graduate student of Chongqing Medical University majoring in clinical laboratory diagnosis. Her research interest is the development of biosensing strategy for clinical diagnosis.

Xiaolong Gou is currently a graduate student of Chongqing Medical University majoring in clinical laboratory diagnosis. His research interest is the development of biosensing strategy for clinical diagnosis.

Min Zhao is a postdoctor of College of Laboratory Medicine, Chongqing Medical University. She received her PhD from College of Chemistry and Chemical Engineering, Southwest University in 2017. Her research subject is the fabrication of metal nanoclusters for pharmaceutical and biomedical analysis.

Shijia Ding is currently a professor of Chongqing Medical University majoring in clinical laboratory diagnosis. His research interest is the development of biosensing strategy for clinical laboratory diagnosis.

Wei Cheng obtained his M.D. degree in clinical laboratory diagnosis from Chongqing Medical University in 2011. He is currently a professor in The Center for Clinical Molecular Medical detection, The First Affiliated Hospital of Chongqing Medical University. His research interest is the development of biosensing strategy for clinical laboratory diagnosis.